PERGAMON

International Journal of Solids and Structures 40 (2003) 6633–6651

INTERNATIONAL JOURNAL OF SOLIDS and STRUCTURES

www.elsevier.com/locate/ijsolstr

The coupled effects of plastic strain gradient and thermal softening on the dynamic growth of voids

X.Y. Wu [a,*], K.T. Ramesh [a], T.W. Wright [a,b]

[a] *Department of Mechanical Engineering, The Johns Hopkins University, Baltimore, MD 21218, USA*
[b] *US Army Research Laboratory, Aberdeen Proving Ground, MD 21005, USA*

Received 13 March 2003; received in revised form 14 July 2003

Abstract

This paper examines the combined effects of temperature, strain gradient and inertia on the growth of voids in ductile fracture. A dislocation-based gradient plasticity theory [J. Mech. Phys. Solids 47 (1999) 1239, J. Mech. Phys. Solids 48 (2000) 99] is applied, and temperature effects are incorporated. Since a strong size-dependence is introduced into the dynamic growth of voids through gradient plasticity, a cut-off size is then set by the stress level of the applied loading. Only those voids that are initially larger than the cut-off size can grow rapidly. At the early stages of void growth, the effects of strain gradients greatly increase the stress level. Therefore, thermal softening has a strong effect in lowering the threshold stress for the unstable growth of voids. Once the voids start rapid growth, however, the influence of strain gradients will decrease, and the rate of dynamic void growth predicted by strain gradient plasticity approaches that predicted by classical plasticity theories.

1. Introduction

Ductile fracture in many metals begins with the nucleation of voids from foreign particles (by brittle cracking or decohesion of particles) or other defects. Voids then grow through plastic deformation of the surrounding medium. The growth of a number of voids eventually leads to void coalescence and ductile fracture. The relics of the voids are still observed on the fracture surface, so that ductile fracture is typically characterized by a dimpled fracture surface.

Foreign particles contained in a typical metal usually have various sizes from tens or hundreds of nanometers (such as carbide particles) to a few tens of micrometers (such as large sulphides and oxides). Experiments indicate that there is not enough sulphide or oxide inclusions to account for the numerous large cavities found at typical fracture surfaces (Baucer and Wilsdorf, 1973; Faleskog and Shih, 1997). It appears that some of the large voids might have originated from very small foreign particles, like carbides,

* Corresponding author. Present address: Department of Surgery and Biomedical Engineering, Emory University, Room 5105 WMB, 1639 Pierce Drive, Atlanta, GA 30322, USA. Tel.: +1-404-727-8274; fax: +1-404-727-3660.
E-mail address: xwu2@emory.edu (X.Y. Wu).

0020-7683/$ - see front matter © 2003 Elsevier Ltd. All rights reserved.
doi:10.1016/S0020-7683(03)00439-6

or from preexisting cavities. Small-angle neutron scattering and TEM experiments have found that cavities on the order of tens of nanometers exist in metal alloys (Page et al., 1984; Zakaria and Munroe, 2002). When cavities grow from tens or hundreds of nanometers to tens or hundreds of micrometers, the matrix material surrounding voids must experience extremely large plastic deformations and strong gradients of plastic strains then exist due to geometry. Recently, many convincing experiments, mainly from micro-indentation or nano-indentation (Ma and Clarke, 1995; Nix and Gao, 1998; Shu and Fleck, 1998; Swadener et al., 2002), have shown that materials display strong size effects, when the characteristic length scale associated with non-uniform plastic deformation is on the order of microns. Classical plasticity theories do not have an intrinsic material length scale and thus fail to capture this strong size dependency of material behaviors. Several strain gradient plasticity theories have been proposed to address this problem. Among them, a physics-oriented model is strain gradient plasticity based on dislocation theory, which has been introduced by Gao, Huang and coworkers (Gao et al., 1999; Huang et al., 2000). This dislocation-based strain gradient plasticity approach will be adopted in this paper.

On the micron or submicron scales, the effect of strain gradient has been found to significantly increase the stress level for the unstable growth of voids (Fleck and Hutchinson, 1997; Huang et al., 2000). This significant increase of stress could result in much more plastic work being done. Since thermal softening is related to the amount of plastic work dissipated as heat, it could become a more important issue for void growth with strain gradient plasticity, as compared to the fairly weak effects of thermal softening predicted by classical plasticity theories (Cortes, 1992b; Tong and Ravichandran, 1993, 1995). Therefore, it is worthwhile incorporating temperature effects into strain gradient plasticity. Because of the influence of temperature on the dislocation densities, it is convenient to incorporate temperature effects in the framework of dislocation-based strain gradient plasticity theory.

In addition to the effects of strain gradient and temperature, the effect of inertia is another key to understanding void growth. Since Carroll and Holt's pioneering work (Carroll and Holt, 1972), it has been recognized that inertia stabilizes the growth of voids (Cortes, 1992a,b; Ortiz and Molinari, 1992; Tong and Ravichandran, 1995; Wang, 1994a,b; Worswick and Pick, 1995). In a prior work (Wu et al., 2003a), we have extended Ortiz and Molinari's single spherical void model (Ortiz and Molinari, 1992) and adopted the concept of the critical stress from cavitation instability (Huang et al., 1991) to examine the effects of inertia, rate dependency and temperature on void growth. We found that the effects of inertia dominate the growth of the void in the long term so that the void growth rate becomes independent of the initial size shortly after the applied stress exceeds the critical stress. This result sheds new insight on the observed morphology of fracture surfaces. Because strain gradient effects may greatly increase the critical stress level for the unstable growth of voids, we will reexamine the effect of inertia on void growth in the framework of strain gradient plasticity.

In this paper, we incorporate thermal softening into dislocation-based strain gradient plasticity and reconstruct the constitutive laws. Then, we examine the combined effects of strain gradients and adiabatic thermal softening on the critical stress for the unstable growth of voids. Finally, numerical calculations are performed to study void growth with the combined effects of inertia, thermal softening, heat conduction and strain gradient.

2. Constitutive laws for strain gradient plasticity

In this section, we start with the Taylor relation and incorporate a thermal effect into strain gradient plasticity. Next, we reconstruct the constitutive law based on the multiscale approach proposed by Gao, Huang and coworkers (Gao et al., 1999; Huang et al., 2000). Finally, we describe the conservation of energy, following the kinematics of deformation. Throughout the paper, the material is assumed to be

homogenous, isotropic and plastically incompressible. Because the plastic deformation region is limited, linear elasticity is explicitly included in the calculations.

2.1. Incorporation of thermal softening into strain gradient plasticity

The Taylor relation between the shear strength and dislocation density in a material is

$$\tau = \alpha\mu b\sqrt{\rho_S + \rho_G}, \tag{1}$$

where τ is the shear stress, μ is the shear modulus, b is the Burgers vector, ρ_T is the total dislocation density, ρ_S is the density of statistically stored dislocations, ρ_G is the density of geometrically necessary dislocations, and α is an empirical constant ($\sim$0.3). From the Taylor relation, Gao et al. (1999) then obtained a constitutive function:

$$\sigma = \sigma_Y\sqrt{f^2(\varepsilon) + l\eta}. \tag{2}$$

Here, σ_Y is the yield stress, ε is the effective strain, η is the effective plastic strain gradient (explicitly defined later in this paper), l is the intrinsic material length and $\sigma = \overline{M}\tau$ is the effective stress. $\overline{M}$ (the Taylor factor) is the ratio of tensile flow stress to shear flow stress (for polycrystalline FCC materials $\overline{M} = 3.06$ (Bishop and Hill, 1951a,b)). $f(\varepsilon)$ is a plastic strain-hardening function. The material is assumed to obey power-law plastic strain hardening and linear elasticity so that $f(\varepsilon) = (\varepsilon/\varepsilon_Y)^n$ for $\varepsilon \geqslant \varepsilon_Y$ and $f(\varepsilon) = \varepsilon/\varepsilon_Y$ for $\varepsilon \leqslant \varepsilon_Y$.

In the absence of a strain gradient ($\eta = 0$ so that $\rho_G = 0$), the density of statistically stored dislocations ρ_S can be expressed in terms of the strain-hardening function $f(\varepsilon)$:

$$\rho_S = (\sigma_Y f(\varepsilon) - \sigma_Y)^2/(\overline{M}\alpha\mu b)^2. \tag{3}$$

Geometrically necessary dislocations appear in the strain gradient field for compatible deformation. Arsenlis and Parks (1999) have constructed a relation between the density of geometrically necessary dislocations ρ_G and the effective plastic strain gradient η.

$$\rho_G = \lambda\eta/b, \tag{4}$$

where λ is Nye's factor (in polycrystalline FCC materials, $\lambda = 1.85$ for torsion and $\lambda = 1.93$ for bending). Using Eq. (4) in (1) and then comparing with (2), one obtains the intrinsic material length as

$$l = \overline{M}^2\alpha^2(\mu/\sigma_Y)^2\lambda b. \tag{5}$$

For example, for polycrystalline FCC metals in the bending case this material length scale would be $l \approx 18\alpha^2(\mu/\sigma_Y)^2 b$. For non-uniform plastic deformations, the effects of plastic strain gradient are important when the characteristic length associated with the deformation becomes comparable to the intrinsic material length l. For most structural engineering materials, the intrinsic material length is on the order of microns (for very pure metals, l could be orders of magnitude larger). Therefore, the effect of plastic strain gradient may be an important issue in the problem of growth of microvoids (on the order of microns or smaller).

Up to this point, all of our discussions are based on the isothermal assumption. However, our application of interest is dynamic void growth under dynamic loading, and during high rate plastic deformations, the temperature may rise to a significant fraction of the melting temperature, and significant thermal softening may occur. We therefore seek to incorporate thermal effects into the model. The influence of temperature on material strength is typically obtained from uniaxial tension or compression experiments. For simplicity, we assume that the effects of thermal softening and strain hardening may be written as follows:

$$\sigma = \sigma_Y \cdot h_1(T^*) \cdot f(\varepsilon). \tag{6}$$

Here, T^* is the temperature rise (room temperature is taken as the reference), and $h_1(T^*)$ is a thermal softening function. Then, the density of statistically stored dislocations in Eq. (3) can be rewritten to include the effect of temperature:

$$\rho_S = (\sigma_Y f(\varepsilon) - \sigma_Y)^2 \cdot h_1^2(T^*)/(\overline{M}\alpha\mu b)^2. \tag{7}$$

Eq. (7) includes the influence of temperature on recovery: thermal energy facilitates the motion and annihilation of dislocations so that the dislocation density will be reduced because of the temperature rise. In the description of dislocation densities in Eq. (1), we separated the dislocations into two different categories, statistically stored dislocations and geometrically necessary dislocations, in terms of their different generation mechanisms. However, it appears reasonable to assume that thermal softening results in the recovery of both types of dislocation. Following Eq. (7), we rewrite the density of geometrically necessary dislocations ρ_G as

$$\rho_G = \lambda\eta \cdot h_2^2(T^*)/b, \tag{8}$$

where $h_2(T^*)$ is a second thermal softening function characterizing the temperature dependency of ρ_G. The temperature dependency of ρ_G could perhaps be examined using micro- or nano-indentation experiments at different temperatures, but this is beyond the scope of this study. With thermal softening taken into account, the constitutive law (2) for strain gradient plasticity is modified to give

$$\sigma = \sigma_Y\sqrt{f^2(\varepsilon) \cdot h_1^2(T^*) + l\eta \cdot h_2^2(T^*)} = \sigma_Y h(T^*)\sqrt{f^2(\varepsilon) + l\eta}, \tag{9}$$

where the thermal softening has been assumed to have the same form for ρ_G and $\rho_S : h_2(T^*) = h_1(T^*) = h(T^*)$ to simplify the problem. In the region of elastic deformations only, thermo-elasticity is applied

$$\sigma = \sigma_Y \cdot h(T^*) \cdot \varepsilon/\varepsilon_Y. \tag{10}$$

On the elastic–plastic boundary ($\varepsilon = \varepsilon_Y$ so that $f(\varepsilon) = 1$), the continuity of the effective stress indicates the effective plastic strain gradient should be zero.

2.2. Mechanism-based strain gradient plasticity

Gao, Huang and coworkers (Gao et al., 1999; Huang et al., 2000) proposed a multiscale approach to construct the constitutive laws, the equilibrium equations and the boundary conditions for strain gradient plasticity. A modified decomposition of the strain gradient tensor was proposed by Jiang et al. (2002), because a pure volumetric strain results in a deviatoric strain gradient in Gao and Huang's original decomposition. Following the same approach, we reconstruct the constitutive equations for strain gradient plasticity, incorporating the effect of temperature:

$$\sigma_{ik} = K\delta_{ik}\varepsilon_{pp} + \frac{2\sigma}{3\varepsilon}\varepsilon'_{ik} \tag{11}$$

and

$$\tau_{ijk} = l_\varepsilon^2\left(KH_{ijk} + \sigma\Phi_{ijk} + \frac{\sigma_Y^2 h^2(T^*)}{\sigma}\Psi_{ijk}\right), \tag{12}$$

where

$$\Phi_{ijk} = \frac{1}{\varepsilon}(\Lambda_{ijk} - \Pi_{ijk}), \quad \Psi_{ijk} = f(\varepsilon)f'(\varepsilon)\Pi_{ijk}, \quad \varepsilon = \sqrt{\frac{2}{3}\varepsilon'_{ij}\varepsilon'_{ij}}, \quad \eta = \frac{1}{2}\sqrt{\eta'_{ijk}\eta'_{ijk}}, \tag{13}$$

$$\Lambda_{ijk} = \left[2\eta'_{ijk} + \eta'_{kij} + \eta'_{kji}\right] \Big/ 72, \tag{14}$$

$$\Pi_{ijk} = \left[\varepsilon'_{ik}\eta'_{jmn} + \varepsilon'_{jk}\eta'_{imn}\right] \cdot \varepsilon'_{mn} \Big/ 54\varepsilon^2, \tag{15}$$

$$H_{ijk} = \frac{1}{24}\left[\delta_{ik}\eta_{jpp} + \delta_{jk}\eta_{ipp}\right], \tag{16}$$

$$\sigma = \sigma_{\mathrm{Y}} h(T^*)\sqrt{f^2(\varepsilon) + l\eta} \tag{17}$$

and

$$\eta'_{ijk} = \eta_{ijk} - \eta^H_{ijk}, \quad \eta^H_{ijk} = \frac{1}{3}\left(\varepsilon_{pp,j}\delta_{ik} + \varepsilon_{pp,i}\delta_{jk} - \varepsilon_{pp,k}\delta_{ij}\right). \tag{18}$$

Here K is the bulk modulus, $\varepsilon_{ij} = (u_{i,j} + u_{j,i})/2$ are the strains, $\varepsilon'_{ij} = \varepsilon_{ij} - \delta_{ij}\varepsilon_{pp}/3$ are the deviatoric strains, η'_{ijk} is the deviator of the strain gradient $\eta_{ijk} = u_{k,ij}$, and τ_{ijk} are the higher order stresses which are work conjugate to the strain gradient η_{ijk}.

The new length parameter $l_\varepsilon = \beta(\mu/\sigma_{\mathrm{Y}})b$ introduced in Eq. (12) is called the mesoscale cell size and characterizes the transition from standard plasticity to gradient plasticity. The constant β is suggested (Huang et al., 2000) to take values between 1 and 10. Bazant (2002) argues that the asymptotic behavior at small sizes is unreasonably strong in Gao and Huang's dislocation-based strain gradient plasticity. One suggestion is that the third-order stresses τ_{ijk} be eliminated, corresponding to $l_\varepsilon = 0$ (or $\beta = 0$). We will vary β from 0 to 10 to examine the influence of the mesoscale cell size in our specific problem of void growth.

In formulating the above constitutive laws, we assume that the temperature is uniform within the mesoscale "cell". If temperature is not uniform, the third-order stresses τ_{ijk} would be affected while the second-order stresses σ_{ij} remain unaffected. If the size of the mesoscale cell is sufficiently small (compared with the intrinsic material length l), the influence of temperature gradient on the third-order stress is negligible. Otherwise, the influence of temperature gradient on the third-order stress has to be considered, which we leave to future investigation.

The equilibrium equation is given by

$$\sigma_{ik,i} - \tau_{ijk,ij} + f_k = 0, \tag{19}$$

where f_k is the body force. The traction boundary condition is

$$t_k = n_i\left(\sigma_{ik} - \tau_{ijk,j}\right) - D_j\left(n_j\tau_{ijk}\right) + D_k\left(n_i n_j n_p \tau_{ijp}\right) + \left(n_i n_j \tau_{ijk} - n_k n_i n_j n_p \tau_{ijp}\right)(D_q n_q). \tag{20}$$

Here, n_i is the unit normal to the surface and $D_j = (\delta_{jp} - n_j n_p)\frac{\partial}{\partial x_p}$ is the surface gradient operator. When the principle of virtual work is applied to obtain the equilibrium equation in strain gradient plasticity, an additional traction appears due to the existence of the third-order stress:

$$s_k = n_i n_j \tau_{ijk} - n_k n_i n_j n_p \tau_{ijp}. \tag{21}$$

Note this additional traction s_k acts only on the boundary where the traditional traction t_k is applied, and in the case where only traction boundary conditions are applied and the surface of the body is smooth, or in the case where only displacement boundary conditions are applied, this additional traction condition will disappear. For the problem of spherical void growth that we consider, the additional traction boundary condition in (21) disappears as only traction boundary conditions are applied (traction free on the void surface) and the surfaces of the body are smooth (spherical).

When the material is only elastically deformed, the equilibrium Eq. (19) reduces to

$$\sigma_{ik,i} + f_k = 0 \tag{22}$$

with ordinary traction boundary conditions

$$t_k = n_i \sigma_{ik}. \tag{23}$$

Note that there is no plastic strain gradient, and therefore, no third-order stress in the elastic region. On the elastic–plastic boundary, the third-order stresses disappear, but their derivatives may still exist. Thus, an inconsistency may arise if we apply the equilibrium equations (19) and (22) or apply the boundary conditions (20) and (23) to the elastic–plastic boundary at the same time. This possible inconsistency can be avoided if the third-order stresses can be neglected as Bažant suggested, which corresponds to $l_\varepsilon = 0$ in Eq. (12).

2.3. Kinematics

Consider an infinite medium containing a spherical void and subjected to a remote far-field hydrostatic loading as shown in Fig. 1. As the far-field loading p^{app} is increased, the surface of the void yields first, and then the elastic–plastic boundary (denoted as r_c) propagates outwards. This problem is essentially a 1-D problem and the deformation is accordingly described by

$$r = r(R, t), \tag{24}$$

where r and R are the radii in the current and undeformed configurations respectively. We use A to denote the initial void radius, and a to denote the current void radius. If we assume elastic–plastic incompressibility, this requires

$$r^3 - R^3 = a^3 - A^3. \tag{25}$$

The particle velocity can then be expressed in terms of the velocity of the void surface

$$v_r = \dot{\boldsymbol{r}} = a^2 \dot{\boldsymbol{a}} / r^2. \tag{26}$$

It follows that the rates of deformation in the current configuration are

$$D_{rr} = \mathrm{d}v_r/\mathrm{d}r = -2a^2\dot{\boldsymbol{a}}/r^3, \quad D_{\theta\theta} = D_{\phi\phi} = v_r/r = a^2\dot{\boldsymbol{a}}/r^3. \tag{27}$$

After integrating with respect to time, the strains can be obtained as

$$\varepsilon_{rr} = -2\varepsilon_{\theta\theta} = -2\varepsilon_{\phi\phi} = -2\ln(r/R). \tag{28}$$

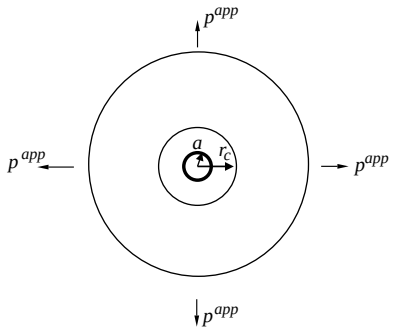

Fig. 1. Schematic diagram of the spherical model: an infinite body contains a single spherical void and is subjected to a remote hydrostatic tensile loading. Once the void surface yields, the elastic–plastic boundary (denoted by its radius, r_c) propagates outwards. r_c divides the whole region into two parts: the inner elastic–plastic region and the outer purely elastic region.

The rates of the strain gradient are given in terms of the rate of deformation by

$$\begin{aligned} &\dot{\eta}_{rrr} = \partial D_{rr}/\partial r, \quad \dot{\eta}_{\theta\theta r} = \partial D_{\theta\theta}/\partial r, \quad \dot{\eta}_{\phi\phi r} = \partial D_{\phi\phi}/\partial r, \\ &\dot{\eta}_{r\theta\theta} = \dot{\eta}_{\theta r\theta} = (D_{rr} - D_{\theta\theta})/r, \quad \dot{\eta}_{r\phi\phi} = \dot{\eta}_{\phi r\phi} = (D_{rr} - D_{\phi\phi})/r \end{aligned} \tag{29}$$

and the strain gradients are then

$$\eta_{\theta\theta r} = \eta_{\phi\phi r} = \eta_{r\theta\theta} = \eta_{\theta r\theta} = \eta_{r\phi\phi} = \eta_{\phi r\phi} = -\eta_{rrr}/2 = -3(1/R - 1/r). \tag{30}$$

Using the definition in (18b), the hydrostatic part of the strain gradient is $\eta^H_{ijk} = 0$, because of the incompressibility $\varepsilon_{pp} = 0$. Then, the effective strain and the effective strain gradient become

$$\varepsilon = 2\ln(r/R), \quad \eta = 3\sqrt{5/2}(1/R - 1/r). \tag{31}$$

Setting $\varepsilon = \varepsilon_Y$, we obtain the elastic–plastic boundary r_c (in the current configuration). Once the void grows sufficiently large ($a^3 \gg A^3$), the position of the elastic–plastic boundary can be approximated as $r_c/a = (\frac{2}{3\varepsilon_Y})^{1/3}$. The effective strain gradient can also be calculated on the elastic–plastic boundary and is denoted as η_0. Note that η_0 represents the gradient of the elastic strain. There is no plastic deformation, so that there are no geometrically necessary dislocations on the elastic–plastic boundary. Therefore, we should subtract the gradient of elastic strain from the total effective strain gradient η when we calculate the effective stresses from Eq. (9) in the plastic zone. Otherwise, the effective stress calculated from elasticity would be inconsistent with that calculated using strain gradient plasticity. In this work, η_0 is uniformly subtracted from the effective strain gradient in the plastic zone as a first-order approximation.

2.4. Conservation of energy

During plastic deformation, most of the plastic work is dissipated in the form of heat, which results in a local temperature rise and softening of material. The plastic work increment per unit volume is

$$\mathrm{d}w = \sigma'_{ij}\,\mathrm{d}\varepsilon'_{ij} + \tau'_{ijk}\,\mathrm{d}\eta'_{ijk}. \tag{32}$$

Here, $\sigma'_{ij} = \sigma_{ij} - \sigma^H_{ij}$ and $\tau'_{ijk} = \tau_{ijk} - \tau^H_{ijk}$ are the deviatoric parts of the second- and third-order stresses, respectively. The first term on the right hand side in Eq. (11) represents the hydrostatic part of the second-order stresses σ^H_{ij}. Similarly, the counterpart in Eq. (12) represents the hydrostatic part of the third-order stresses τ^H_{ijk}. Eq. (32) shows that plastic work is done not only by the second-order stresses against plastic strain but also by the third-order stresses against the plastic strain gradient.

For this spherically symmetric problem, the conservation of energy requires

$$\rho C_p\,\mathrm{d}T^* = \frac{k}{r^2}\frac{\partial}{\partial r}\left(r^2\frac{\partial T^*}{\partial r}\right)\mathrm{d}t + \zeta\,\mathrm{d}w, \tag{33}$$

where ρ is the density of the material, C_p is the specific heat at constant pressure, k is the thermal conductivity, t is the time, and ζ is a coefficient representing the fraction of plastic work transformed into heat (assumed to be 0.9 in our case). The left hand side of Eq. (33) represents the rate (per unit volume) of the energy needed to increase the temperature by $\mathrm{d}T^*$. On the right hand side, the first term represents the amount of heat conducted away in time $\mathrm{d}t$, and the second term is the rate of plastic work converted into heat. In the localized region near the surface of the void, the rate of plastic work is very high, and therefore, the temperature rise may be very high. If the heat is being conducted away sufficiently quickly, the temperature in the matrix material will be uniformly low, and the influence of thermal softening on void growth will be negligible. In contrast, if the heat cannot be conducted away sufficiently quickly, the temperature in the matrix near the surface of the void will build up and the temperature rise might affect the growth of the void.

A diffusion length is typically associated with heat conduction, and characterizes how far heat can be conducted away in a given time-period. However, heat is only generated in the plastic zone. Therefore, if the thermal diffusion length is much smaller than the size of the plastic zone, the effect of heat conduction on void growth will be negligible; if it is much larger, the thermal diffusion will conduct heat away sufficiently quickly and the effect of thermal softening on void growth will be negligible. A scaling law is used to illustrate the length dependency of the influence of heat conduction on void growth. The dimensionless temperature rise $\widetilde{T}$ and the dimensionless radius $\tilde{r}$ are defined as

$$\widetilde{T}^* = T^* \cdot c, \quad \tilde{r} = r/a, \tag{34}$$

where c is the thermal softening coefficient and a the current void size. Eq. (33) can now be rewritten in terms of the scaled quantities as

$$\frac{\rho C_p}{c} \cdot \mathrm{d}\widetilde{T}^* = \frac{k}{a^2 c} \cdot \frac{1}{\tilde{r}^2} \frac{\partial}{\partial \tilde{r}} \left(\tilde{r}^2 \frac{\partial \widetilde{T}^*}{\partial \tilde{r}} \right) \cdot \mathrm{d}t + \zeta \cdot \mathrm{d}w. \tag{35}$$

Eq. (35) indicates that the influence of heat conduction strongly depends on the current void size. The smaller the void is, the stronger the influence of heat conduction on void growth. The length and time dependency of the influence of heat conduction on void growth has been thoroughly explored in our previous study Wu et al. (2003b), where the effect of strain gradient is absent. In this paper, the length dependence of the influence of heat conduction coupled with the effect of strain gradient is examined through numerical simulations.

3. Effect of strain gradient on void growth

In this section, we first calculate the threshold stresses for the unstable growth of voids both in the athermal and in the adiabatic cases, with a view toward addressing the dependence of the threshold stress on the intrinsic material length. Next, we simulate the dynamic growth of voids and examine the combined effects of inertia, thermal softening, heat conduction and strain gradient on void growth.

3.1. Effect of strain gradient on instability of void growth

In spherical coordinates, the equilibrium equation (19) in the plastic deformation region reads

$$\begin{aligned} &\frac{\mathrm{d}\sigma_{rr}}{\mathrm{d}r} + \frac{2(\sigma_{rr} - \sigma_{\theta\theta})}{r} - \frac{\mathrm{d}}{\mathrm{d}r}\left[\frac{\mathrm{d}\tau_{rrr}}{\mathrm{d}r} + \frac{2}{r}(\tau_{rrr} - \tau_{r\theta\theta} - \tau_{\theta\theta r}) \right] - \frac{2}{r}\left[\frac{\mathrm{d}}{\mathrm{d}r}(\tau_{rrr} - \tau_{r\theta\theta}) \right. \\ &\left. + \frac{1}{r}(2\tau_{rrr} - 5\tau_{r\theta\theta} - 3\tau_{\theta\theta r}) \right] = 0. \end{aligned} \tag{36}$$

The equilibrium equation (22) in the elastic region can also be rewritten in spherical coordinates,

$$\frac{\mathrm{d}\sigma_r}{\mathrm{d}r} + \frac{2(\sigma_{rr} - \sigma_{\theta\theta})}{r} = 0. \tag{37}$$

A free traction boundary is applied to the surface of the void, and a dead-load boundary is applied at infinity ($\sigma_r = p^{\mathrm{app}}$). The loading history is shown in Fig. 2: a remote loading is applied at a constant rate to a given level p_{S} in a rise time t_{R}, and is then held steady for a time t_{h}. After integrating Eqs. (36) and (37), one may obtain the applied stress for void growth, which is balanced by the resistant stress:

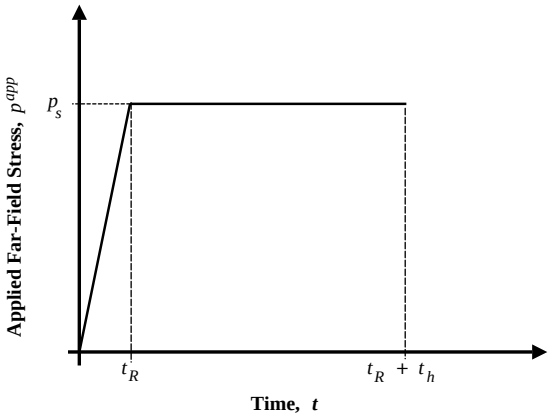

Fig. 2. History of applied far-field loading. Initially the load increases at a constant loading rate until the end of the rise-time t_R, and is then held steady at magnitude p_S for an additional time t_h.

$$p^{\text{app}} = p^{\text{res}} = 2\int_{r_c}^{\infty} \frac{\sigma_{\theta\theta} - \sigma_{rr}}{r}\,\mathrm{d}r + 2\int_{a}^{r_c} \left\{ \frac{\sigma_{\theta\theta} - \sigma_{rr}}{r} + \frac{3(\tau_{rrr} - 2\tau_{r\theta\theta} - \tau_{\theta\theta r})}{r^2} \right\} \mathrm{d}r. \tag{38}$$

Here p^{res} represents the resistance of the matrix material surrounding the void to the expansion of the void through elastic and plastic deformation. We obtain the second- and third-order stresses using the constitutive laws developed in Section 2.2, and using the strains and strain gradients calculated in Section 2.3.

$$\begin{aligned}
&\sigma_e = \sigma_Y h_1(T^*)\omega, \quad \omega = \sqrt{f^2(\varepsilon) + l(\eta - \eta_0)},\\
&\tau_{rrr} = \frac{\sqrt{2} l_\varepsilon^2 \sigma_Y h_1(T^*)}{9\sqrt{5}} \cdot \frac{f(\varepsilon) f'(\varepsilon)}{\omega} \cdot (\eta - \eta_0),\\
&\tau_{\theta\theta r} = \tau_{\phi\phi r} = -\frac{l_\varepsilon^2 \sigma_Y h_1(T^*)}{9\sqrt{10}} \cdot \frac{\omega}{\varepsilon} \cdot (\eta - \eta_0),\\
&\tau_{r\theta\theta} = \tau_{r\phi\phi} = \tau_{\theta r\theta} = \tau_{\phi r\phi} = -\frac{l_\varepsilon^2 \sigma_Y h_1(T^*)}{18\sqrt{10}} \cdot \left(\frac{\omega}{\varepsilon} + \frac{f(\varepsilon) f'(\varepsilon)}{\omega} \right) \cdot (\eta - \eta_0).
\end{aligned} \tag{39}$$

Here, η is the effective strain gradient and η_0 the effective strain gradient on the elastic–plastic boundary. Using (39) in Eq. (38), and noting that $\sigma_e = \sigma_{\theta\theta} - \sigma_{rr}$ and $\int_{r_c}^{\infty} \frac{\sigma_e}{r}\,\mathrm{d}r = \frac{\sigma_Y}{3}$ (from the linear elastic solution), the resistant stress is given by

$$p^{\text{res}} = \frac{2}{3}\sigma_Y + 2\sigma_Y \int_{\bar{a}}^{\bar{r}_c} \frac{h_1 \omega}{\bar{r}}\,\mathrm{d}\bar{r} + \frac{2\sigma_Y}{3\sqrt{10}} \cdot \left(\frac{l_\varepsilon}{l}\right)^2 \cdot \left(\frac{l}{A}\right)^2 \cdot \int_{\bar{a}}^{\bar{r}_c} \frac{h_1}{\bar{r}^2} \cdot \left(\frac{2\omega}{\varepsilon} + \frac{3 f(\varepsilon) f'(\varepsilon)}{\omega} \right) \cdot (\bar{\eta} - \bar{\eta}_0)\,\mathrm{d}\bar{r}. \tag{40}$$

Here, we normalize R, r, l, a, r_c, η and η_0 by the initial void size A so that $\bar{R} = R/A$, $\bar{r} = r/A$, $\bar{l} = l/A$, $\bar{a} = a/A$, $\bar{r}_c = r_c/A$, $\bar{\eta} = \eta \cdot A$ and $\bar{\eta}_0 = \eta_0 \cdot A$. Note that the third term on the right hand side in Eq. (40) is proportional to the square of the mesoscale cell size l_ε, so that the resistant stress depends on the mesoscale cell size. However, the mesoscale cell size to intrinsic material length ratio ($l_\varepsilon/l = \beta\sigma_Y/18\alpha^2\mu$) is typically very small. Therefore, an appreciable effect of the mesoscale cell size on the resistant stress is only expected at large l/A ratios. Also note that, for any given l/A ratio, the integral $\int_{\bar{a}}^{\bar{r}_c} \frac{h_1}{\bar{r}^2} \cdot \left(\frac{2\omega}{\varepsilon} + \frac{3 f(\varepsilon) f'(\varepsilon)}{\omega}\right) \cdot (\bar{\eta} - \bar{\eta}_0)\,\mathrm{d}\bar{r}$ approaches zero as the void grows to infinity (this has been checked through numerical computations).

That is, if the void becomes sufficiently large, the dependence of the resistant stress on the mesoscale cell size will be negligible. A thorough examination of these issues is obtained through the numerical simulations that we describe next, addressing the dependence of void growth on the resistant stress when the intrinsic material length, mesoscale cell size and temperature are considered.

Fig. 3 represents the resistant stresses plotted against the relative growth of the void, in both the athermal (solid line) and adiabatic (dotted line) conditions. The material properties correspond to maraging steel and its thermo-mechanical properties are presented in Table 1. The intrinsic material length to initial void size ratio is fixed at $l/A = 20$ so that the void is initially considerably smaller than the material length scale, and the parameter β is fixed at $\beta = 1.0$ (Table 1). The plots show that, as the void begins to grow, the resistant stress p^{res} initially increases but then reaches a maximum and begins to drop once the relative void growth (a/A) exceeds a critical value (which is typically less than 3); for the specific case of the athermal condition, Huang et al. (2000) obtained similar results. The maximum value of the resistant stress is defined as a "threshold stress" for the unstable growth of the void. If the applied stress exceeds this threshold stress and the effect of inertia is not considered, the void can grow without bound. Once the relative void growth (a/A) exceeds the critical value, the resistant stress begins to decrease as the void continues to expand, and eventually saturates at the critical stress for the unstable growth of void predicted by the classical plasticity theory (corresponding to the $l/A = 0$ case in gradient plasticity). Thus, once the void has expanded to a

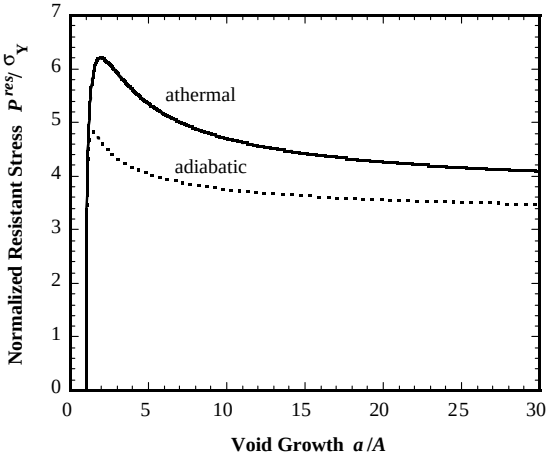

Fig. 3. The applied stresses versus the relative growth of void both in the athermal (represented by the solid line) and adiabatic (represented by dotted line) condition. The material properties correspond to maraging steel with $\sigma_Y = 1760$ MPa and $\mu = 73$ GPa, while other thermo-mechanical properties are presented in Table 1. The intrinsic material length to initial void size ratio is fixed at $l/A = 20$, and the parameter β is fixed at $\beta = 1.0$.

Table 1
Material properties of maraging steel

Shear's modulus (GPa)	Yield stress (MPa)	Yield strain	Strain-hardening exponent	Specific heat (kJ/kg K)	Conductivity (W/m K)	Density (kg/m^3)	Thermal softening coefficient (1/K)
73	1760	0.008	0.01	480[a]	25.3	8.0×10^3	0.001

[a] Data from www.matweb.com.

sufficiently large size, the surrounding material exhibits a constant resistance to the further expansion of the void. This has important implications in the dynamic growth of voids, as we discuss in the next section.

Fig. 3 shows that thermal softening greatly decreases the resistant stress, because the hardening effect of the plastic strain gradient significantly increases the stress level at this large l/A ratio. This results in a larger amount of plastic work being developed during void growth, and this results in a higher local temperature rise.

Fig. 4 considers the dependence of the calculated threshold stress (normalized by the yield stress) on the intrinsic material length to initial-void-size ratio, for the athermal and adiabatic conditions and for three different values of the parameter β ($\beta = 0, 1, 10$). The material considered in these simulations remains the maraging steel used in the simulations of Fig. 3, with an intrinsic material length of around 1.4 μm. Note that changes in β correspond to changes in the mesoscale cell size l_e, with the limit $\beta = 0$ corresponding to the third-order stress being neglected. Both in the athermal and adiabatic conditions, the threshold stresses in the $\beta = 1$ case are almost identical to those in the $\beta = 0$ case, and no dependency of threshold stress on mesoscale cell size is observed. This is consistent with our previous asymptotic analysis that showed that no appreciable dependency of threshold stress on mesoscale cell size is expected unless the l/A ratio is sufficiently large (how large depends on l_e/l and so on β). In the $\beta = 1$ case, the maximum value of the l/A ratio of 40 considered here is not large enough to display the influence of the mesoscale cell size on the threshold stress. However, if the parameter β is increased to 10, the threshold stresses begin to be significantly increased immediately after the l/A ratio reaches about 10. When the l/A ratio is less than 10, the threshold stress is insensitive to the mesoscale cell size for $\beta = 0$–10. This result is consistent with the result obtained by Huang et al. (2000) in the athermal case. Note that the limit $l/A = 0$ corresponds either to classical plasticity or to a sufficiently large initial void size.

Fig. 4 reveals the strong dependence of the threshold stress on the l/A ratio. As the initial void size A decreases, so that l/A increases to about 40, the threshold stress increases by 10% in the $\beta = 0$ case and by 300% in the $\beta = 10$ case. The dependence of threshold stress on l/A ratio indicates that there does not exist a critical stress for cavitation instability in the strain gradient theory, because the threshold stress is infinite for an infinitesimal void. The unlimited growth of voids requires the surmounting of the threshold stress by the applied stress. Therefore, the magnitude of a given applied loading will determine a critical value of initial void size (called the cut-off size in this paper)—any void that is initially smaller than this cut-off size will stop growing after a very limited growth under the given applied stress.

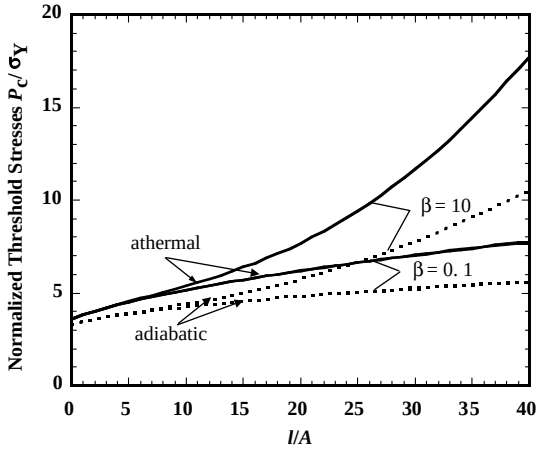

Fig. 4. The threshold stresses versus the l/A ratios for three cases: $\beta = 0, 1, 10$, both in the athermal (solid lines) and adiabatic (dotted lines) conditions. The material is the same as in Fig. 3.

Examining the adiabatic results in Fig. 4, we see that the effects of thermal softening on the threshold stress are much stronger in the $\beta = 10$ case than in the $\beta = 0$ case, for the same reasons described previously in the discussion of Fig. 3.

3.2. Effect of strain gradient on dynamic void growth

Up to this point, we have not considered the effect of inertia, which is a key issue in the problem of void growth. When the effect of inertia is taken into account, the equation of motion in the plastic deformation region becomes

$$\frac{\mathrm{d}\sigma_{rr}}{\mathrm{d}r}+\frac{2(\sigma_{rr}-\sigma_{\theta\theta})}{r}-\frac{\mathrm{d}}{\mathrm{d}r}\left[\frac{\mathrm{d}\tau_{rrr}}{\mathrm{d}r}+\frac{2}{r}(\tau_{rrr}-\tau_{r\theta\theta}-\tau_{\theta\theta r})\right]-\frac{2}{r}\left[\frac{\mathrm{d}}{\mathrm{d}r}(\tau_{rrr}-\tau_{r\theta\theta})+\frac{1}{r}(2\tau_{rrr}-5\tau_{r\theta\theta}-3\tau_{\theta\theta r})\right]=\rho\ddot{r}. \tag{41}$$

In the purely elastic region, this reduces to

$$\frac{\mathrm{d}\sigma_{rr}}{\mathrm{d}r}+\frac{2(\sigma_{rr}-\sigma_{\theta\theta})}{r}=\rho\ddot{r}. \tag{42}$$

The incompressibility of material implies that the particle acceleration can be determined in terms of the velocity and acceleration of particles on the void surface ($r = a$):

$$\ddot{r}=\frac{\mathrm{d}}{\mathrm{d}r}\left(\frac{a^2\ddot{a}}{r}+\frac{2a\dot{a}^2}{r}-\frac{a^4\dot{a}^2}{2r^4}\right). \tag{43}$$

Integrating Eqs. (41) and (42) with respect to the current radius r, one readily obtains,

$$p^{\mathrm{app}}-\rho\left(a\ddot{a}+\frac{3}{2}\dot{a}^2\right)=p^{\mathrm{res}}, \tag{44}$$

where the resistant stress p^{res} is defined in Eq. (40). Comparing this with Eq. (38), the additional term on the left hand side in (44) represents the effect of inertia. In the absence of strain gradient effects, all voids (even with different initial sizes) tend to achieve a constant rate of growth, due to the dominating effect of inertia in the long term (Wu et al., 2003a). In strain gradient plasticity, our analyses in the previous section show that the right-hand side in (44) encounters a maximum value (the threshold stress) when the void approximately triples its size (Fig. 3), and that the threshold stress greatly increases as the initial void size decreases (Fig. 4). Further, without the effect of inertia, the stress level of a given applied loading determines a cut-off size. In this section we use numerical simulations to determine whether the effect of inertia changes the cut-off size. The combined effects of thermal softening and heat conduction on dynamic void growth are also examined through numerically solving the equation of motion (44) and the conservation of energy (33).

In the problem of void growth, both our scaling asymptotic analysis and numerical calculations indicate that even if the dependence of the resistant stress on mesoscale cell size is negligible once the void grows sufficiently large, the influence of mesoscale cell size on threshold stress could be extremely strong at extremely small sizes. In the following simulations of dynamic void growth (including inertia), therefore, we will take $\beta = 0$ as Bažant suggested. The effect of temperature is still included since thermal softening could greatly lower the threshold stress even in the $\beta = 0$ case.

The numerical calculations are performed for the same maraging steel in the athermal, adiabatic and diffusive conditions, using the loading history that is described in Fig. 2 (the loading rate is 10 GPa/μs with the final loading level fixed at $6.2\sigma_{\mathrm{Y}}$). Fig. 5 compares the computed dynamic growth of voids (in the

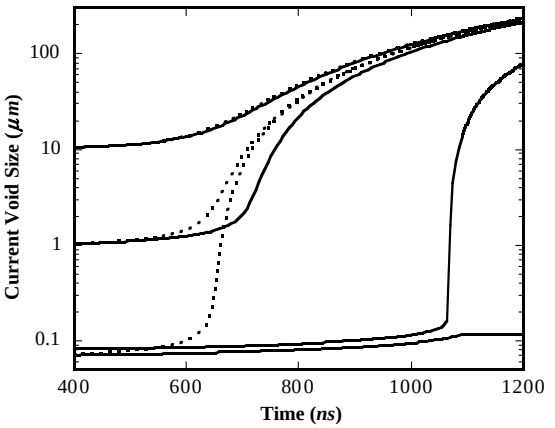

Fig. 5. Current void sizes versus time. The solid lines represent the dynamic growth of voids predicted by the theory of strain gradient plasticity, while the dotted lines represent the dynamic growth predicted by the classical plasticity. The material remains to be maraging steel with intrinsic material length $l = 1.4$ μm and the final applied loading level is $6.2\sigma_Y$. The effect of temperature is not included.

athermal condition) that is predicted by the strain gradient plasticity theory and classical plasticity theory for four specific initial void sizes: $A = 10$, 1 μm, 80, and 70 nm. The solid lines represent the current void sizes as predicted by the strain gradient plasticity theory, while the dotted lines represent the current void sizes predicted by classical plasticity. In the $A = 10$ μm case, the inclusion of the strain gradients does not affect the dynamic growth of the void significantly because the initial void size is already much larger than the intrinsic material length l of 1.4 μm. When the initial void size is on the order of the intrinsic material length, as in the $A = 1$ μm case, an appreciable delay of the void growth is observed due to the effect of the strain gradient. The effect of strain gradient becomes far more significant when the initial void sizes are reduced to submicrons, and the existence of the cut-off size can be seen in Fig. 5. The earlier non-inertial calculation showed that for a loading of $6.2\sigma_Y$ the cut-off size would be 0.07 μm. When the inertia is included, Fig. 5 shows that a 0.07 μm void expands and then stops growing (the growth stops once the applied load stops increasing and is held steady). In contrast, a 0.08 μm void can grow without bound. This indicates that the cut-off size in the inertial case is a number between 0.07 and 0.08 μm for this applied loading, and that the effect of inertia does not appreciably change the cut-off size.

As the void grows, the resistant stress p^{res} eventually saturates (Fig. 3) at a stress that corresponded to the critical stress (denoted as p_{cr}) for the unstable growth of voids, and predicted by the classical plasticity theory. Once the resistant stress p^{res} saturates at p_{cr}, one obtains an asymptotic solution to Eq. (44):

$$\dot{a}_e = \sqrt{2(p^{app} - p_{cr})/3\rho}. \tag{45}$$

Eq. (45) implies that voids will achieve a constant "equilibrium" rate $\dot{a}_e$ that depends only on the degree of supercriticality $(p^{app} - p_{cr})$ and not on the void size. This is essentially identical to the result obtained in our previous study (Wu et al., 2003a) in the absence of a strain gradient effect. Thus, the dynamic growth in the strain gradient and non-strain gradient cases will eventually achieve the same "equilibrium rate". However, there is a significant difference between these two cases. In the non-strain gradient case, the dynamic growth of all voids eventually achieves the equilibrium growth rate under supercritical loading; in contrast, in the strain gradient case, only those voids whose initial sizes are greater than the cut-off size can achieve this equilibrium growth rate.

Fig. 5 shows that there is a significant delay of dynamic void growth in the 0.08 μm case. This is because the threshold stresses are different for voids with different initial sizes, and for a given rate of applied

loading, the times needed to surmount the threshold stress are different. For example, the threshold stress is around $6.0\sigma_Y$ for a 0.08 μm void, while the critical stress for cavitation instability predicted by the classical plasticity theory is $3.6\sigma_Y$. Therefore, classical plasticity predicts that all voids will start to grow without bound immediately after the applied stress exceeds $3.6\sigma_Y$. However, strain gradient plasticity implies that no appreciable growth occurs until the applied stress exceeds $6.0\sigma_Y$ in the 0.08 μm case. As the applied loading rate in these calculations is 10 GPa/μs and the yield stress is $\sigma_Y = 1760$ MPa, it takes 400 additional nanoseconds to reach the $6.0\sigma_Y$ threshold stress in the 0.08 μm case (i.e., 400 ns after the time when the applied stress reaches the $3.6\sigma_Y$ critical stress predicted by the classical plasticity theory). Thus, the effect of strain gradient will result in a substantial delay (more than 400 ns) of growth in the 0.08 μm case, as shown in Fig. 5.

Thermal effects on the dynamic growth of voids under strain gradient plasticity are shown in Fig. 6, where the adiabatic (dotted lines) and thermally diffusive (solid lines) growth histories of voids are presented for various initial void sizes. When the initial void size is 10 μm, the thermally diffusive and adiabatic void growth histories are nearly identical. This negligible influence of heat conduction on dynamic void growth for large initial voids was demonstrated in our previous work (Wu et al., 2003b) based on non-gradient plasticity. In the 1 μm case, an appreciable delay of the dynamic void growth is observed in the thermally diffusive case as compared with the adiabatic case. When the initial size goes down to 0.1 μm, an even larger delay of void growth is observed in the thermally diffusive case. This indicates that heat can be conducted away sufficiently quickly from the inner hot region near the void surface when the initial void size is on the order of hundreds of nanometers. Thus, the threshold stress will be larger in the thermally diffusive condition than in the adiabatic condition (Fig. 4 shows that the adiabatic threshold stress is appreciably lower than the athermal threshold stress). It thus takes longer to surmount the threshold stress in the thermally diffusive case than in the adiabatic case, resulting in the delay of the *diffusive* growth of voids. Further, since the threshold stress increases in the thermally diffusive condition due to heat conduction, the cut-off size described in Fig. 5 also increases. Fig. 6 shows that in the adiabatic condition a 0.03 μm void will grow while a 0.02 μm void will not, so that the adiabatic cut-off size is between 0.02 and 0.03 μm, whereas the cut-off size is between 0.05 and 0.06 μm in the thermally diffusive case. Thus, the cut-off size in the thermally diffusive case is close to that in the athermal case (between 0.07 and 0.08 μm, as shown in Fig. 5).

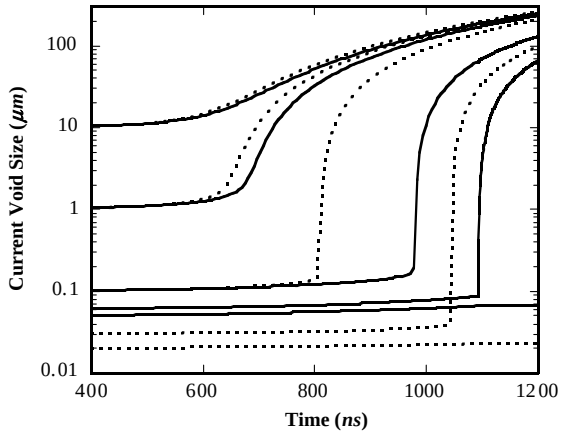

Fig. 6. Current void sizes versus time. The dotted lines represent the thermally adiabatic growth of voids, while the solid lines represent the thermally diffusive growths. The effect of strain gradient is included.

4. Discussion

Many micro-indentation and nano-indentation hardness experiments (Ma and Clarke, 1995; Nix and Gao, 1998; Shu and Fleck, 1998; Swadener et al., 2002) have shown the strong effects of strain gradients on plastic deformation. However, there is little direct experimental evidence of the effects of strain gradients on void growth. Analytical and numerical results in this paper and other literature (Fleck and Hutchinson, 1997; Huang et al., 2000) have demonstrated that the effects of strain gradients greatly raise the stress level required for the unstable growth of voids. This could have important implications for ductile fracture, which the following two micrographs of the fracture surfaces of copper might help to illustrate.

Our previous study (Wu et al., 2003b) shows that the influence of thermal softening is much stronger for maraging steel with respect to other materials, so that the numerical simulations have been performed on maraging steel in the previous section in order to better demonstrate the combined effects of thermal softening and strain gradient. This discussion section will be focused on micrographs of the fracture surfaces of copper, not only because the experimental evidence available on maraging steel is limited but also the relatively weak influence of thermal softening for copper (Wu et al., 2003b) helps to single out the effect of strain gradient on ductile fracture (thermal softening lowers the critical stress 0.6 GPa in maraging steel, but only 0.1 GPa in copper). The influence of thermal softening and thermal diffusion will be discussed in more detail in this section.

Fig. 7a is a micrograph taken from the fracture surface in OFHC copper in ductile spallation (Zurek et al., 1988). The duration of the loading pulse is on the order of a microsecond. Suppose that the applied loading is over the critical stress for the unstable growth of void growth predicted by the classical plasticity theory (otherwise, the growth of voids will be very limited so that ductile failure will not take place in this experiment). According to our previous study in the absence of strain gradient (Wu et al., 2003a), voids of all sizes achieve the same "equilibrium" growth rate under supercritical loading and rapidly tend toward similar final sizes regardless of their initial sizes. The applied loading level, the critical stress and the material density determine the equilibrium growth rate, $\dot{a}_e = \sqrt{2(p^{app} - p_{cr})/3\rho}$. The critical stress for the unstable growth of voids depends on the material properties, such as the yield stress, the yield strain and the strain-hardening exponent (Wu et al., 2003b); the critical stress in copper is typically 1–2 GPa depending on purity, prior plastic work etc. (the spall strength quoted by Zurek et al. is 2.4 GPa). Therefore, the "equilibrium" growth rate will reach tens of micrometers per microsecond if the applied stress is over the critical stress by more than a few percent. Thus, the duration of the loading pulse (on the order of a microsecond) is long enough for all voids to grow to similar final sizes, of the order of 10 μm. Fig. 7a shows that the majority of voids on the fracture surface are around 8 μm with some smaller ones about 2 or 3 μm.

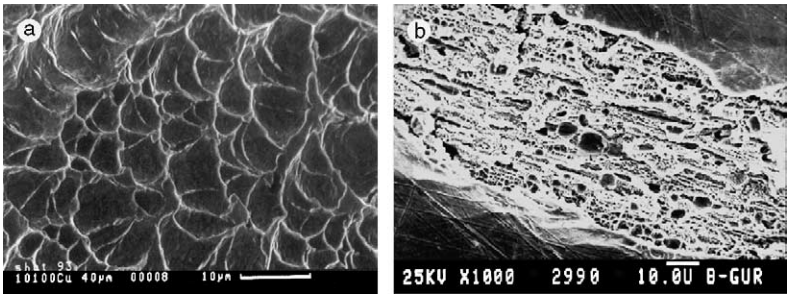

Fig. 7. (a) Voids on the fracture surface in OFHC copper (after Zurek et al., 1988) developed in a plate impact experiment. (b) Microvoids on the fracture surface in copper (after Moshe et al., 1998) developed during a laser shock experiment.

Fig. 7b shows the fracture surface (Moshe et al., 1998) of a specimen made of annealed copper that was forced to spall using a laser shock approach (now the pulse duration is only 2.2 ns). The spall strength in this case was stated to be 9 GPa. The morphology of the fracture surface is now significantly different from that of Fig. 7a. The number of voids observed on the fracture surface increases significantly, while the void sizes greatly decrease. The majority of voids on the fracture surface are around 1 or 2 μm, while a small number of voids are 4 or 5 μm in size. Factors that may contribute to the different morphologies of fracture surfaces observed in Fig. 7a and b include the effects of heat conduction, rate dependency, void interaction, strain gradients and void nucleation. We consider each of these in turn.

The influence of heat conduction on dynamic void growth strongly depends on the void size and the rate of void growth (Wu et al., 2003b). At the early stages of void growth, heat can be more easily conducted away from the surface of smaller voids so that heat conduction retards the growth of smaller voids compared with that of bigger ones. However, the effect of heat conduction is appreciable only when the adiabatic critical stresses are appreciably lower than the athermal critical stress, such as in 4340 steels and maraging steels. Thermal softening does not greatly lower the critical stress in copper due to the low strength of the material (Wu et al., 2003b). Further, when the applied stress is much higher than the critical stress as in Fig. 7b, all voids start rapid, adiabatic growth according to the classical plasticity theory. Therefore, heat conduction cannot account for the morphology of the final fracture surface shown in Fig. 7b.

Rate dependence can strongly delay the growth of smaller voids especially in the early stages of void growth (Wu et al., 2003a). The effect of rate dependence on dynamic void growth becomes greater as the rate sensitivity of the material increases (Wu et al., 2003a), and pure annealed copper is a rate sensitive material. Thus, rate dependence can result in a more non-uniform distribution of void sizes the higher loading rate and shorter pulse durations of Fig. 7b (compared with the relatively uniform distribution of void sizes at lower loading rate and longer pulse duration in Fig. 7a). However, rate dependence cannot account for the many more voids that appear on the fracture surface of Fig. 7b, because the rate sensitivity of a material does not affect the critical stress for the unstable growth of voids (Wu et al., 2003a).

Void interaction can accelerate the dynamic growth of voids (and has stronger effects on the big voids) when the volume fraction of voids becomes high (Wu, 2002). However, void interaction has little influence on the void growth in the early stages, and does not affect the number of voids that grow; thus void interactions cannot explain the increased number density of voids observed in Fig. 7b.

The two remaining factors, the effects of strain gradient and void nucleation, can both account for the increased number density of voids observed in Fig. 7b. We consider the strain gradient effects first.

Because of the effect of strain gradients, the threshold stress for the unstable growth of voids depends strongly on the initial void size if the initial size is smaller than the intrinsic material length (the threshold stress increases as the initial void size decreases). For any given applied load level, there will exist an initial void size below which the threshold stress for void growth will be greater than the applied stress, so that voids below this initial size will not grow. In this sense, in strain gradient plasticity the stress level of the applied loading determines the cut-off size for the rapid growth of voids. Voids cannot grow to visible sizes if their initial sizes are less than this cut-off size. If the applied stress level is higher (as in the laser shock case of Fig. 7b compared with the plate impact case of Fig. 7a), the cut-off size will be smaller so that more voids will be expected on the fracture surface (as is observed). In Fig. 7b, the applied loading level is 9 GPa and the duration of the loading pulse is 2.2 ns. According to Eq. (45), voids in the laser shock experiment will achieve an "equilibrium" growth rate between 520 and 770 μm/μs (corresponding to critical stresses of 2 and 1 GPa). At these rates of growth, voids are expected to achieve 1–2 μm in 2.2 ns. Most of the voids observed on the fracture surface are around 2 μm. Noting that void interactions may accelerate the growth of the voids, the analytical prediction of void size is consistent with the experimental observation. As the voids grow, the influence of strain gradient on dynamic void growth decreases, and in the long term, the

effects of inertia will dominate void growth and all voids tend toward similar final sizes. However, if the loading is not held long enough, as in the laser shock case, the effects of strain gradients will result in a wider distribution of void sizes. Thus, consideration of the effects of strain gradients can account for the larger numbers of voids and the smaller average void sizes in the fracture surface of Fig. 7b compared with Fig. 7a.

Substantially increased void nucleation at high stresses is another factor that could account for the morphology of the fracture surface in Fig. 7b. Void nucleation at small second phase particles is more difficult than that at larger second phase particles (Argon et al., 1975), because the energetic "cost" to form new surface has to be compensated by the elastic strain energy released from the second phase particle when the separation of the interface takes place. At higher stresses, more voids can be nucleated since more elastic strain energy is available. However, it is possible that in spallation experiments the kinetic energy that is available can also compensate the energetic "cost" to form new surface. Further, Pardoen et al. (1998) suggest that the interface between inclusions and the matrix in pure copper is very weak so that voids can be easily nucleated even at low stresses. If this is the case, then the effects of strain gradients on void growth may be responsible for the appearance of the fracture surface in Fig. 7b. This remains circumstantial evidence, and further research is required to obtain experimental verification of strain gradient effects in the void growth problem.

5. Summary

We have constructed constitutive laws that incorporate the effects of thermal softening for strain gradient plasticity, and applied this modified theory to address the combined effects of temperature and plastic strain gradients on the dynamic growth of voids. The study focuses on the dependence of the void growth on two length scales introduced in the strain gradient plasticity theory: the intrinsic material length $l = 18\alpha^2(\mu/\sigma_Y)^2 b$ and the mesoscale cell size $l_\varepsilon = \beta(\mu/\sigma_Y)b$.

When the initial void size A is smaller than the intrinsic material length l ($l/A \gg 1$), we confirm that the effects of strain gradient greatly increase the threshold stress for the unstable growth of voids, and find that thermal softening has strong effects in lowering the threshold stress. When the ratio of the intrinsic material length to the initial void size is greater than 10, our numerical simulations show strong dependence of the threshold stress on the mesoscale cell size. Our numerical results show the threshold stress in the $\beta = 10$ case is much higher than that in the $\beta = 0$ case when the initial void size is small ($l/A > 10$) (values of β between 1 and 10 are typically suggested). Thus, we take $\beta = 0$ when we examine the effects of strain gradient on dynamic void growth.

Because the threshold stress increases as the initial void size decreases, a cut-off size is then set by the stress level of the applied loading. If the initial sizes of voids are smaller than this cut-off size, voids will stop growing when the applied loading is held steady. If the initial sizes of voids are larger than the cut-off size, the rapid growth of voids takes places when the applied loading surmounts the corresponding threshold stresses. This suggests that more voids should appear on the fracture surface at a higher applied loading. As the voids grow, the influence of strain gradient on dynamic void growth decreases. In the long term, the effects of inertia will dominate void growth and all voids tend toward similar final sizes. However, if the loading is not held long enough or the loading rate is not high enough, the effects of strain gradients will result in a wider distribution of void sizes.

At the early stages of void growth, the effects of strain gradients greatly increase the stress and so the effects of thermal softening on dynamic void growth become more important. Thermal softening and heat conduction both affect the cut-off size of voids. Heat conduction also delays the rapid growth of voids and the effects of heat conduction increases as the initial void sizes decrease.

Acknowledgements

This work was performed under the auspices of the Center for Advanced Metallic and Ceramic Systems (CAMCS) at Johns Hopkins. This research was sponsored by the Army Research Laboratory (ARMAC-RTP) and was accomplished under ARMAC-RTP Cooperative Agreement Number DAAD19-01-2-0003.

References

Argon, A.S., Im, J., Safoglu, R., 1975. Cavity formation from inclusions in ductile fracture. Metall. Trans. 6A, 825–837.

Arsenlis, A., Parks, D.M., 1999. Crystallographic aspects of geometrically-necessary and statistically-stored dislocation density. Acta Mater. 47, 1597–1611.

Baucer, R.W., Wilsdorf, H.G.F., 1973. Void initiation in ductile fracture. Scripta Meter. 7, 1213–1220.

Bazant, Z.P., 2002. Scaling of dislocation-based strain-gradient plasticity. J. Mech. Phys. Solids 50, 435–448.

Bishop, J.F.W., Hill, R., 1951a. A theoretical derivation of the plastic properties of polycrystalline face-centered metal. Philos. Mag. 42, 1298–1307.

Bishop, J.F.W., Hill, R., 1951b. A theory of plastic distortion of a polycrystalline aggregate under combined stresses. Philos. Mag. 42, 414–427.

Carroll, M.M., Holt, A.C., 1972. Static and dynamic pore-collapse relations for ductile porous materials. J. Appl. Phys. 43, 1626–1636.

Cortes, R., 1992a. Dynamic growth of microvoids under combined hydrostatic and deviatoric stresses. Int. J. Solids Struct. 29, 1637–1645.

Cortes, R., 1992b. The growth of microvoids under intense dynamic loading. Int. J. Solids Struct. 29, 1339–1350.

Faleskog, J., Shih, C.F., 1997. Micromechanics of coalescence—i. Synergistic effects of elasticity, plastic yielding and multi-size-scale voids. J. Mech. Phys. Solids 45, 21–50.

Fleck, N.A., Hutchinson, J.W., 1997. Strain gradient plasticity. Adv. Appl. Mech. 33, 295–361.

Gao, H., Huang, Y., Nix, W.D., Hutchinson, J.W., 1999. Mechanism-based strain gradient plasticity—i. Theory. J. Mech. Phys. Solids 47, 1239–1263.

Huang, Y., Hutchinson, J.W., Tvergaard, V., 1991. Cavitation instabilities in elastic–plastic solids. J. Mech. Phys. Solids 39, 223–241.

Huang, Y., Gao, H., Nix, W.D., Hutchinson, J.W., 2000. Mechanism-based strain gradient plasticity—ii. Analysis. J. Mech. Phys. Solids 48, 99–128.

Jiang, H., Huang, Y., Guo, T.F., Hwang, K.C., 2002. An alternative decomposition of the strain gradient tensor. J. Appl. Mech. 69, 139–141.

Ma, Q., Clarke, D.R., 1995. Size dependent hardness of silver single crystals. J. Mater. Res. 10, 853–863.

Moshe, E., Eliezer, S., Dekel, E., Ludmirsky, A., Henis, Z., Werdiger, M., Eliaz, N., Eliezer, D., 1998. An increase of the spall strength in aluminum, copper, and metglas at strain rates larger than 10^7 s^{-1}. J. Appl. Phys. 83, 4004–4011.

Nix, W.D., Gao, H., 1998. Indentation size effects in crystalline materials: a law for strain gradient plasticity. J. Mech. Phys. Solids 46, 411–425.

Ortiz, M., Molinari, A., 1992. Effect of strain hardening and rate sensitivity on the dynamic growth of a void in a plastic material. J. Appl. Mech. 59, 48–53.

Page, R.A., Lankford, J., Spooner, S., 1984. Small-angle neutron scattering study of creep cavity nucleation and growth in sintered alumina. J. Mater. Sci. 19, 3360–3374.

Pardoen, T., Doghri, I., Delannay, F., 1998. Experimental and numerical comparison of void growth models and void coalescence criteria for the prediction of ductile fracture in copper bars. Acta Mater. 46, 541–552.

Shu, J.Y., Fleck, N.A., 1998. The prediction of a size effect in micro-indentation. Int. J. Solids Struct. 35, 1363–1383.

Swadener, J.G., George, E.P., Pharr, G.M., 2002. The correlation of the indentation size effect measured with indenters for various shapes. J. Mech. Phys. Solids 50, 681–694.

Tong, W., Ravichandran, G., 1993. Dynamic pore collapse in viscoplastic materials. J. Appl. Phys. 74, 2425–2435.

Tong, W., Ravichandran, G., 1995. Inertial effects on void growth in porous viscoplastic materials. Trans. ASME: J. Appl. Mech. 62, 633–639.

Wang, Z.P., 1994a. Growth of voids in porous ductile materials at high strain rate. J. Appl. Phys. 76, 1535–1542.

Wang, Z.-P., 1994b. Void growth and compaction relations for ductile porous materials under intense dynamic general loading conditions. Int. J. Solids Struct. 31, 2139–2150.

Worswick, M.J., Pick, R.J., 1995. Void growth and coalescence during high velocity impact. Mech. Mater. 19, 293–309.

Wu, X.Y., 2002. The Dynamic Growth of Voids in Viscoplastic Materials. Ph.D. Dissertation. The Johns Hopkins University.

Wu, X.Y., Ramesh, K.T., Wright, T.W., 2003a. The dynamic growth of a single void in a viscoplastic material under transient hydrostatic loading. J. Mech. Phys. Solids 51, 1–26.

Wu, X.Y., Ramesh, K.T., Wright, T.W., 2003b. The effects of thermal softening and heat conduction on the dynamic growth of voids. Int. J. Solids Struct. 40, 4461–4478.

Zakaria, M., Munroe, P.R., 2002. Void formation and morphology in NiAl. J. Meter. Sci. 37, 71–79.

Zurek, A.K., Johnson, J.N., Frantz, C.E., 1988. Characterization of dynamic fracture in copper under uniaxial stress and uniaxial strain. J. Phys. France Colloq. C3 (DYMAT 88) 49, 269–276.